Remote Sensing in Ecology and Conservation
Open Access
ZSL LET'S WORK FOR WILDLIFE

ORIGINAL RESEARCH

Target-oriented habitat and wildlife management: estimating forage quantity and quality of semi-natural grasslands with Sentinel-1 and Sentinel-2 data

Christoph Raab[1,2], Friederike Riesch[1,2], Bettina Tonn[1,2], Brian Barrett[3], Marcus Meißner[4], Niko Balkenhol[2,4,5] & Johannes Isselstein[1,2,4]

[1]Grassland Science, Faculty of Agricultural Science, University of Goettingen, Von-Siebold-Str. 8, 37075 Goettingen, Germany
[2]Centre of Biodiversity and Sustainable Land Use (CBL), University of Goettingen, Buesgenweg 1, 37077 Goettingen
[3]School of Geographical and Earth Sciences, University of Glasgow, Scotland, United Kingdom
[4]Institut für Wildbiologie Göttingen und Dresden e.V., Buesgenweg 3, 37077 Goettingen, Germany
[5]Wildlife Sciences, Faculty of Forest Sciences and Forest Ecology, University of Goettingen, 37077 Goettingen, Germany

Keywords
Forage quality and quantity, radar, random forest, satellite, semi-natural grassland, Sentinel, variable selection

Correspondence
Christoph Raab, Grassland Science, Faculty of Agricultural Science, University of Goettingen, Von-Siebold-Str. 8, 37075 Goettingen, Germany. Tel: +49 (0)551 395763; Fax: +49 (0)551 399355; E-mail: craab@uni-goettingen.de

Editor: Kate He
Associate Editor: Martin Zlinszky

Received: 25 July 2019; Revised: 28 November 2019; Accepted: 28 January 2020

doi: 10.1002/rse2.149

[Correction added 3 March, after first online publication: the oADF values have been corrected in table 4 in this version]

Abstract

Semi-natural grasslands represent ecosystems with high biodiversity. Their conservation depends on the removal of biomass, for example, through grazing by livestock or wildlife. For this, spatially explicit information about grassland forage quantity and quality is a prerequisite for efficient management. The recent advancements of the Sentinel satellite mission offer new possibilities to support the conservation of semi-natural grasslands. In this study, the combined use of radar (Sentinel-1) and multispectral (Sentinel-2) data to predict forage quantity and quality indicators of semi-natural grassland in Germany was investigated. Field data for organic acid detergent fibre concentration (oADF), crude protein concentration (CP), compressed sward height (CSH) and standing biomass dry weight (DM) collected between 2015 and 2017 were related to remote sensing data using the random forest regression algorithm. In total, 102 optical- and radar-based predictor variables were used to derive an optimized dataset, maximizing the predictive power of the respective model. High R^2 values were obtained for the grassland quality indicators oADF (R^2 = 0.79, RMSE = 2.29%) and CP (R^2 = 0.72, RMSE = 1.70%) using 15 and 8 predictor variables respectively. Lower R^2 values were achieved for the quantity indicators CSH (R^2 = 0.60, RMSE = 2.77 cm) and DM (R^2 = 0.45, RMSE = 90.84 g/m²). A permutation-based variable importance measure indicated a strong contribution of simple ratio-based optical indices to the model performance. In particular, the ratios between the narrow near-infrared and red-edge region were among the most important variables. The model performance for oADF, CP and CSH was only marginally increased by adding Sentinel-1 data. For DM, no positive effect on the model performance was observed by combining Sentinel-1 and Sentinel-2 data. Thus, optical Sentinel-2 data might be sufficient to accurately predict forage quality, and to some extent also quantity indicators of semi-natural grassland.

Introduction

Grassland ecosystems cover approximately 30% of the Earth's terrestrial surface and represent habitats with high biodiversity (Scurlock and Hall 1998; Gibson 2009; Wilson et al. 2012; Dengler et al. 2014; Riesch et al. 2018). The conservation of semi-natural grasslands depends on management, as they originate from human activities, such as livestock grazing or mowing (Peeters et al. 2014). In the last decades, it has become pivotal to actively conserve semi-natural grasslands due to various threats including intensification of land use (Isselstein et al. 2005;

Isselstein 2018), land abandonment (Valkó et al. 2018) and climate change (Lamarque et al. 2014; Dangal et al. 2016). From a conservation perspective, extensive grazing with livestock species and wildlife has become an established and suitable tool to maintain semi-natural grasslands (Van Wieren 1995; Bunzel-Drüke 2008; Rosenthal et al. 2012; Borer et al. 2014). The spatial distribution and activities of large herbivores are affected by the availability and quality of potential forage areas, and so is their impact on the ecosystem through grazing, trampling and dispersion of wastes (Palmer et al. 2003; Catorci et al. 2016; Merkle et al. 2016; Raynor et al. 2016; Fløjgaard et al. 2017). Therefore, spatially explicit information about forage quantity and quality is of critical importance for active grazing management in order to conserve semi-natural grasslands. A timely estimation of forage conditions can, for example, support decisions of supplementary feeding or pasture rotation. In the context of conservation of semi-natural grassland ecosystems, this might include a cost efficient, easy to apply and robust technique to provide timely information about forage quantity and quality. As several components of the forage and not a single parameter seems to influence the grazing behaviour of herbivores, there is a need to consider forage quantity and quality parameters at the same time (Felton et al. 2018). Forage quality depends on a large number of chemical and physical biomass characteristics. Among these, the concentrations of crude protein (CP) and organic acid detergent fibre (oADF, exclusive of residual ash) are particularly useful parameters (Adesogan et al. 2000).

However, collecting field data on forage quantity and quality are a labour-intensive and time-consuming task (Catchpole and Wheeler 1992). Satellite remote sensing offers unique possibilities to evaluate grassland forage quantity and quality for large areas using empirical models (Mutanga et al. 2004; John et al. 2018). For this, regression techniques are used to relate field information to the data recorded by a satellite. Subsequently, these regression models can be applied to the satellite image to predict the grassland forage quantity and quality parameters. Several statistical analysis techniques for the estimation of forage biomass and chemical composition exist (Ali et al. 2016). They include partial least square regression or stepwise multiple linear regression (Ramoelo et al. 2012; Pellissier et al. 2015) and more advanced machine learning techniques, such as random forest (RF) (Breiman 2001; Ramoelo et al. 2015a,b), Artificial Neural Networks (Haykin 1994; Skidmore et al. 2010) or Support Vector Machines (Cortes and Vapnik 1995). RF can be characterized as an ensemble of decision trees, where the prediction is based on the average among all constructed trees. The trees are constructed on bootstrapped training samples and at each split, predictors are randomly sampled. So far, the RF algorithm has most commonly been used for classification (Belgiu and Drăguţ 2016). Other machine learning algorithms, such as Support Vector Machines, or Artificial Neuronal Networks require a more intensive parameter tuning (Wang et al. 2016). The robustness of the RF in a regression context has been confirmed in various studies (e.g. Mutanga et al. (2012) and Ramoelo et al. (2015b)).

For the prediction of biophysical parameters of grassland, several studies have selected important remote sensing variables, such as single bands or vegetation indices (Mutanga et al. 2004; Tong and He 2017; Loozen et al. 2019). Linear-based machine learning approaches, such as lasso and ridge regression, recently showed promising results for the selection of important predictor variables (Zandler et al. 2015). However, non-linear relationships between spectrally derived predictor variables and biophysical response variables can be present (Mutanga et al. 2004; Mutanga and Kumar 2007; Skidmore et al. 2010). When time series data are applied, the correlation between a predictor variable and the respective biophysical variable may change its slope, depending on the phenological phase. In such cases, the non-linear, decision tree-like RF regression algorithm can be superior to linear regression techniques (Strobl et al. 2007; Beckschäfer et al. 2014).

Earth observation sensors with high temporal and spatial coverage can be the preferred choice to establish a robust relationship between samples collected in the field and remotely sensed reflectance data, for example the Moderate Resolution Imaging Spectroradiometer (MODIS) at 250−500 m spatial resolution or the Medium Resolution Imaging Spectrometer (MERIS) at 300−1200 m spatial resolution (Kawamura et al. 2005; Si et al. 2012; Ali et al. 2017b). But the structural and botanical heterogeneity of semi-natural grasslands (Wachendorf et al. 2017; Riesch et al. 2018) may require higher spatial resolutions. This is the case for semi-natural ecosystems, as they are often composed of a mosaic of different landscape features at small scales. Very high resolution satellite systems, such as RapidEye (provides multispectral data at 5 m spatial resolution) or WorldView-2 (records multispectral data at 1.8 m spatial resolution), have been shown to be a valuable data source for estimating biochemical properties of grassland (Ramoelo et al. 2012, 2015b). However, as most of these sensors are operated by commercial companies, this can introduce financial constraints for the application of these data in long-term monitoring for conservation purposes. One freely available alternative could therefore be the medium resolution Operational Land Imager (OLI) sensor (records multispectral data at 30 m spatial

resolution), mounted on the Landsat-8 satellite (Marsett et al. 2006). The Sentinel-2 mission of the European Space Agency provides high (10 m pixel size) to medium (20 and 60 m pixel size) spatial resolution data, combined with a higher spectral (13 bands) and temporal resolution (5 days). This offers a great potential for studying biophysical properties of grassland. Due to the relationship of nitrogen and chlorophyll to the red-edge region of the electromagnetic spectrum (Yoder and Pettigrew-Crosby 1995; Cho and Skidmore 2006; Kokaly et al. 2009), the availability of three red-edge bands covered by the Sentinel-2 sensors was shown to support the mapping of biophysical properties of grassland (Delegido et al. 2011; Frampton et al. 2013; Ramoelo et al. 2015a). Because of the relationship between chlorophyll and nitrogen, the red-edge reflectance may therefore be related to vegetation protein concentration. In particular, Ramoelo et al. (2015a) demonstrated for simulated multispectral Sentinel-2 data that the red-edge and shortwave infrared regions of the electromagnetic spectrum were robust predictors for modelling the spatial distribution of nitrogen and therefore crude protein, in the Lowveld savanna of South-Africa. In addition, Ramoelo and Cho (2018) demonstrated for the same study region that the spatial distribution of nitrogen in the vegetation can be influenced by environmental factors, such as fire frequency or the underlying geological substrate using Sentinel-2 models derived from an analytical spectral device spectrometer. Especially simple ratio-based red-edge indices were shown to have a high potential for mapping nitrogen concentrations (Ramoelo and Cho 2018). On the contrary, Clevers et al. (2017) demonstrated that for agricultural applications on potato fields the Leaf Area Index (LAI) and chlorophyll concentration can be estimated using Sentinel-2 images without red-edge information at 10 m spatial resolution. This was supported by similar findings for an intensive winter wheat cropping system (Delloye et al. 2018). However, the inclusion of red-edge bands increased the predictive power for the estimation of biophysical parameters. Similar results were recently presented by Punalekar et al. (2018) who used Sentinel-2 data to successfully estimate grassland biomass at farm level without including red-edge bands. The results showed a good agreement between compressed sward height (CSH) measurements and the derived biomass maps. In practice, CSH measurements are used to predict available biomass using empirical equations with constant coefficients. Due to changing site conditions over the phenological season, this can introduce a high degree of uncertainty to the prediction (Nakagami and Itano 2014).

In contrast to multispectral data, hyperspectral remote sensing systems draw on the possibilities of the entire electromagnetic spectrum to relate remotely sensed reflectance data to chemical components or the biomass of the vegetation cover (Skidmore et al. 2010; Pellissier et al. 2015). However, hyperspectral satellite or airborne remote sensing data are usually not freely available, which excludes the application of such data for a timely and operational monitoring.

Using a hand-held hyperspectral spectroradiometer, Starks et al. (2004) found that nitrogen and acid detergent fibre concentration can be obtained through the hyperspectral data for monoculture pastures located in the US Great Plains. Recently, Zeng and Chen (2018) showed for a uniform mixture of grass and alfalfa in Montana, USA, that combining canopy reflectance data from different growing stages, measured in the field using a hyperspectral spectroradiometer, was superior over single growing stage models to estimate acid detergent fibre and crude protein concentrations. However, field-based hyperspectral spectroradiometer approaches depend on calibrations obtained from destructive sampling and can be influenced by illumination and site conditions (Perbandt et al. 2010).

All these spectral-based approaches depend of illumination conditions or image acquisitions with a low cloud contamination rate and thus are restricted by weather conditions. Synthetic-aperture radar (SAR) sensors, such as the Sentinel-1 constellation operated by the European Space Agency, can penetrate through clouds and are independent on illumination conditions. SAR systems can provide valuable information about vegetation structure and moisture content in a continuous manner (Barrett et al. 2014; Ali et al. 2016; Wachendorf et al. 2017). With combined ascending and descending orbits of the Sentinel-1 sensors, an even higher temporal resolution compared to that of the optical Sentinel-2 system can provide a continuous data stream, without data gaps due to the presence clouds. In contrast to optical data, SAR systems are not affected by saturation effects in situations of moderate to dense vegetation cover (Huete et al. 2002). The application of SAR data has been successfully tested for agricultural applications in grasslands, such as the detection of mowing events (Voormansik et al. 2013, 2016; Tamm et al. 2016) or the estimation of grassland vegetation height and biomass (Zalite et al. 2016). For agricultural applications, Veloso et al. (2017) demonstrated that (optical) Sentinel-2 and (radar) Sentinel-1 time series data can be related to seasonal dynamics of vegetation by complementing each other. Similar observations were made by Wang et al. (2019) for a mixed grassland located at the US Great Plains. In addition, it was shown that the integration of optical and SAR data can increase the predictive power for grassland biomass (Wang et al. 2019). Thus, the combination of multispectral and SAR remote

sensing data might help to model biophysical properties of semi-natural grassland ecosystems by overcoming the limitations of a single-sensor approach (Dusseux et al. 2014; Wang et al. 2019).

As studies considering grassland forage quantity and quality parameters in synchrony are rare, this study explores the potential advantages of using combined Sentinel-1 and Sentinel-2 data to predict semi-natural grassland biomass, compressed sward height, organic detergent fibre and crude protein concentrations. This will support the management of herbivores by illustrating how timely information of forage conditions can be derived, thus supporting the conservation of semi-natural grassland ecosystems. For this purpose, the random forest regression algorithm was applied on 102 potential predictor variables, including multispectral and SAR indices. The study site was located in the south-east of Germany and is extensively grazed by wild red deer (*Cervus elaphus*) (Riesch et al. 2019). From a methodological point of view, this study was interested in the following research questions:

- Does combining multispectral (Sentinel-2) and radar (Sentinel-1) remote sensing data improve the mapping of semi-natural grassland forage quantity and quality?
- Can an optimized subset of the predictor dataset increase the random forest regression model performance?

Materials and Methods

Study area

The study was carried out in the Grafenwoehr military training area (GTA) located in the south-east of Germany (Bavaria), extending over approximately 230 km² (Fig. 1). GTA is part of the natural region of Upper Palatine-Upper Main Hills, bordering the Franconian Jura in the west, with elevations between 450 and 500 m above sea level. The long-term average temperature and precipitation are 8.3 ± 0.04 °C and 701 ± 4 mm respectively (1981−2010, mean ± SEM, of four weather stations of the German Weather Service (DWD, Deutscher Wetterdienst) in the immediate vicinity). About 40% of GTA is covered with open habitats, such as semi-natural grassland, while forest covers the majority of the area (ca. 60%). Approximately 85% of GTA is part of the Natura 2000 network and contains many rare and highly protected habitat types, forming a refuge for numerous endangered species (Warren and Büttner 2008; Warren et al. 2014). Since 1947, GTA is used as a US Army Garrison. This means that preserving the open landscape is of high importance for military use as well as for maintaining the conservation status of protected open habitat types.

Field data

Various methods exist to assess the quantity of available forage (t'Mannetje 2000). A method, particularly suitable for heterogeneous vegetation is measuring CSH with a rising plate metre (Sanderson et al. 2001; Correll et al. 2003). This measurement can be converted to standing biomass dry weight (DM) based on calibration cuts (Mannetje and Jones 2000).

For this study, the forage quantity and quality dataset provided by the study of Riesch et al. (2019) was used, who investigated the grazing effect of red deer on plot

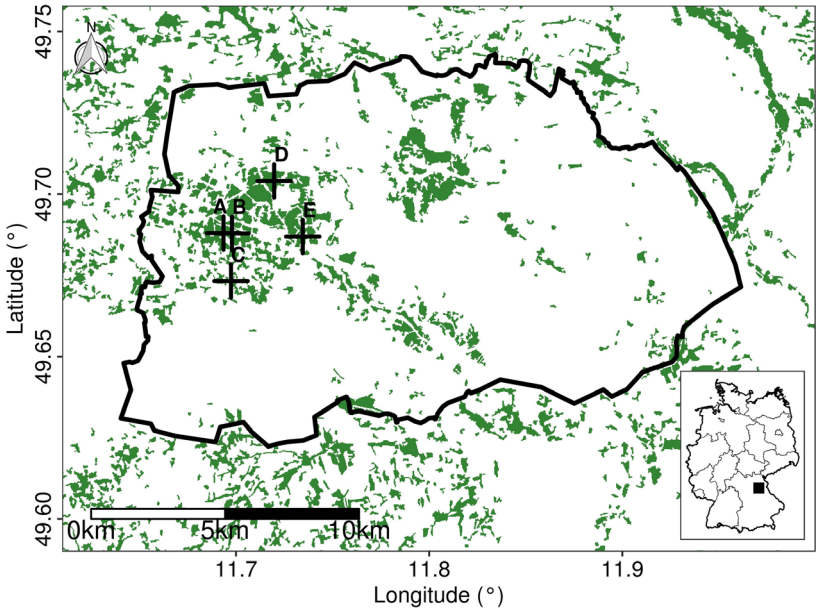

Figure 1. Location of the study site Grafenwoehr Military Training Area. The location of the study site in Germany is highlighted with a black square (lower right corner). The five sampling locations are marked with black crosses and labelled from A-E. The grassland layer is based on data provided by the Copernicus High Resolution Layer: Grassland (GRA) 2015 (© European Union, Copernicus Land Monitoring Service 2018, European Environment Agency (EEA)), illustrated in green.

Figure 2. Photographs from one of the sampling plots at location B in Figure 1. Photographs were taken in (A) May, (B) August and (C) October 2016.

level in GTA covering a 3-year period between 2015 and 2017. This dataset was collected on lowland hay meadows (EU Habitats Directive Annex I habitat type 6510, 'grasslands') in April, May, June, August and October in each of the studied years. At each of the five sampling sites (Fig. 1), three management treatments were compared: grassland was either burnt in late winter/early spring, mown in July or remained untreated. This approximates the spectrum of grassland management activities on GTA and is, therefore, a good representation of the site conditions. Given the five locations and three different treatments, a total of 15 sampling plots with a size of 15 × 15 m each, were included in the dataset. All sampling plots were embedded in a larger, rectangular management treatment area with a mean size of 0.5 ha (sd = 0.1). The mean distance of the sampling plots to the border of the treatment areas was 11.0 m (sd = 4.7). The mean distance between the closest sampling plots was 80.8 m (sd = 42.8). Photographs illustrating one exemplary sampling plot across different phenological phases are shown in Figure 2.

The dataset by Riesch et al. (2019) was collected in five different months over 3 years at five different locations. Each location comprised three plots on different management treatment areas. According to the availability of cloud-free Sentinel-2 data within a time frame of 7 days before and after the respective field sampling, a subset of 120 samples from 8 sampling campaigns were used in the presented study. Details on the respective sampling dates of the utilized dataset are shown in Table 1. For each plot and sampling date, Riesch et al. (2019) determined standing biomass and forage quality values with the following methods: standing biomass was estimated by a double-sampling strategy using CSH measured by a rising plate metre in combination with calibration cuts, that is, above ground biomass cut at ground level on a 0.18 m² area.

The relationship between calibration cut biomass (standing biomass dry weight, DM) and sward height was estimated using a linear model with an average adjusted R^2 of 0.81 (Riesch et al. 2019). Vegetation samples for the analysed forage quality parameters were collected on each sampling date by a hand-pluck approach (Riesch et al. 2019). The total nitrogen concentration in plant material was assessed according to the Dumas combustion method in a carbon nitrogen elemental analyser and subsequently converted to CP.

oADF was determined by near-infrared spectroscopy. Figure 3 gives an overview of the forage quantity and quality parameters provided by the field dataset. The

Table 1. Sampling dates of the dataset provided by Riesch et al. (2019) and corresponding satellite data acquisitions used in this study

Number	Sampling dates	Sensor	Date	Pass
1	2015-06-30–2015-07-02	S1-A	2015-06-26	D
		S1-A	2015-06-29	A
		S2-A	2015-07-04	D
2	2015-08-25–2015-08-26	S1-A	2015-08-21	A
		S1-A	2015-08-25	D
		S2-A	2015-08-26	D
3	2016-05-24–2016-05-26	S2-A	2016-05-22	D
		S1-A	2016-05-23	A
		S1-A	2016-05-27	D
4	2016-08-23–2016-08-24	S1-A	2016-08-19	D
		S1-A	2016-08-22	A
		S2-A	2016-08-27	D
5	2016-10-17–2016-10-20	S2-A	2016-10-16	D
		S1-A	2016-10-18	D
		S1-A	2016-10-21	A
6	2017-05-16–2017-05-17	S1-B	2017-05-16	D
		S2-A	2017-05-17	D
		S1-A	2017-05-18	A
7	2017-08-28–2017-08-30	S2-A	2017-08-25	D
		S1-A	2017-08-29	A
		S1-B	2017-09-01	D
8	2017-10-23–2017-10-25	S1-B	2017-10-22	A
		S1-A	2017-10-25	D
		S2-B	2017-10-29	D

S1, Sentinel-1; S2, Sentinel-2; D, descending orbit; A, ascending orbit.

variability of all parameters increased after June, as cutting lowered DM and CSH, decreased oADF and increased CP concentration in the mown plots (Riesch et al. 2019).

Satellite data and pre-processing

The study used Sentinel-1 and Sentinel-2 imagery for the estimation of semi-natural grassland forage quantity and quality. A conceptual overview of methods applied in this study is presented in Figure 4.

Sentinel-1A (launched on 3 April 2014) and Sentinel-1B (launched on 25 April 2016) satellites are equipped with a C-band synthetic-aperture radar (SAR) with 5.6 cm wavelength (ESA, 2016a). Sentinel-1 level-1 (Ground Range Detected) data collected in the interferometric wide swath mode with dual polarization (VV and VH) were used. This mode has a defined spatial resolution of 5 × 20 m and a geolocation error of 7 m.

Sentinel-2A (launched on 23 June 2015) and Sentinel-2B (launched on 7 March 2017) acquire data in 13 spectral wavelengths with a spatial resolution of 10, 20 and 60 m and a geolocation error of <10 m (Drusch et al. 2012). A detailed overview of the specifications is outlined in Table 2. Since the plot size of field sampling by Riesch et al. (2019) was 15 × 15 m, all analyses were continued with a spatial resolution of 10 m. In addition, all non-grassland areas were masked according to the Copernicus High Resolution Layer with a spatial resolution of 20 m (geolocation error < 10 m): Grassland (GRA) 2015 (© European Union, Copernicus Land Monitoring Service 2018, European Environment Agency (EEA)).

Multispectral data pre-processing

All available level-1C top of atmosphere (TOA) reflectance Sentinel-2 data were acquired from https://scihub.copernicus.eu/dhus/#/home within a temporal window of 7 days before and after the temporal mean of the respective sampling period of Riesch et al. (2019). All images with cloud and cloud-shadow contamination over the sampling sites were subsequently removed from the analysis. The final selection of Sentinel-2 images and the corresponding sampling dates are compiled in Table 1.

The pre-processing included atmospheric and topographic correction using Sen2Cor (Müller-Wilm et al. 2018, version 2.5.5). The Sentinel-2 data were resampled to 10 m spatial resolution using the SNAP software (ESA, 2016b) and the Sen2res resolution enhancement operator provided by Brodu (2017). For the subsequent analyses, all 60 m resolution bands were excluded, as they are mainly designed for atmospheric application purposes.

SAR data pre-processing

Sentinel-1 data were acquired from https://scihub.copernicus.eu/dhus/#/home in descending and ascending orbits as close as possible to the temporal mean of the selected sampling periods of Riesch et al. (2019) (Table 1). The data were pre-processed using SNAP, applying the respective orbit file, geometric calibration, terrain correction, resampling to 10 m spatial resolution using bilinear interpolation and speckle filtering (Lee filter, 3 × 3). Finally, the data were converted to dB using a range-doppler approach.

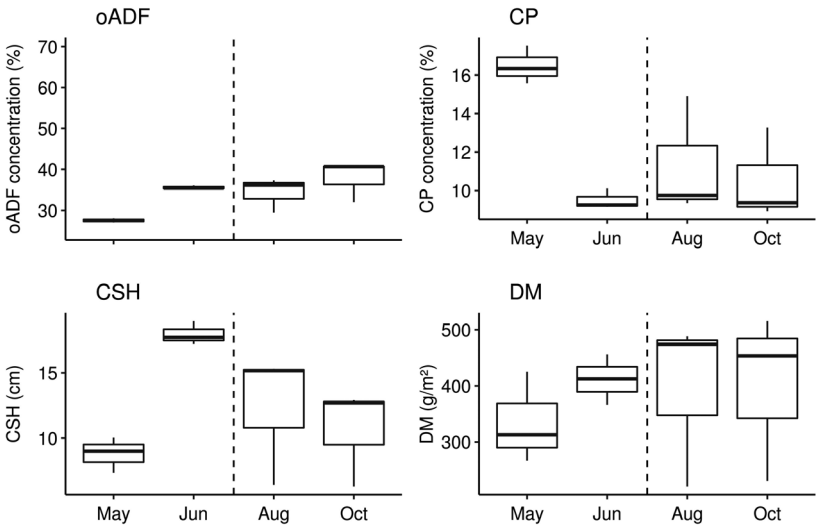

Figure 3. Grassland forage quantity and quality data used in this study (Riesch et al. 2019). The respective sampling dates are shown in Table 1. The cutting events in July are indicated by the dashed line. Abbreviations see Table 3.

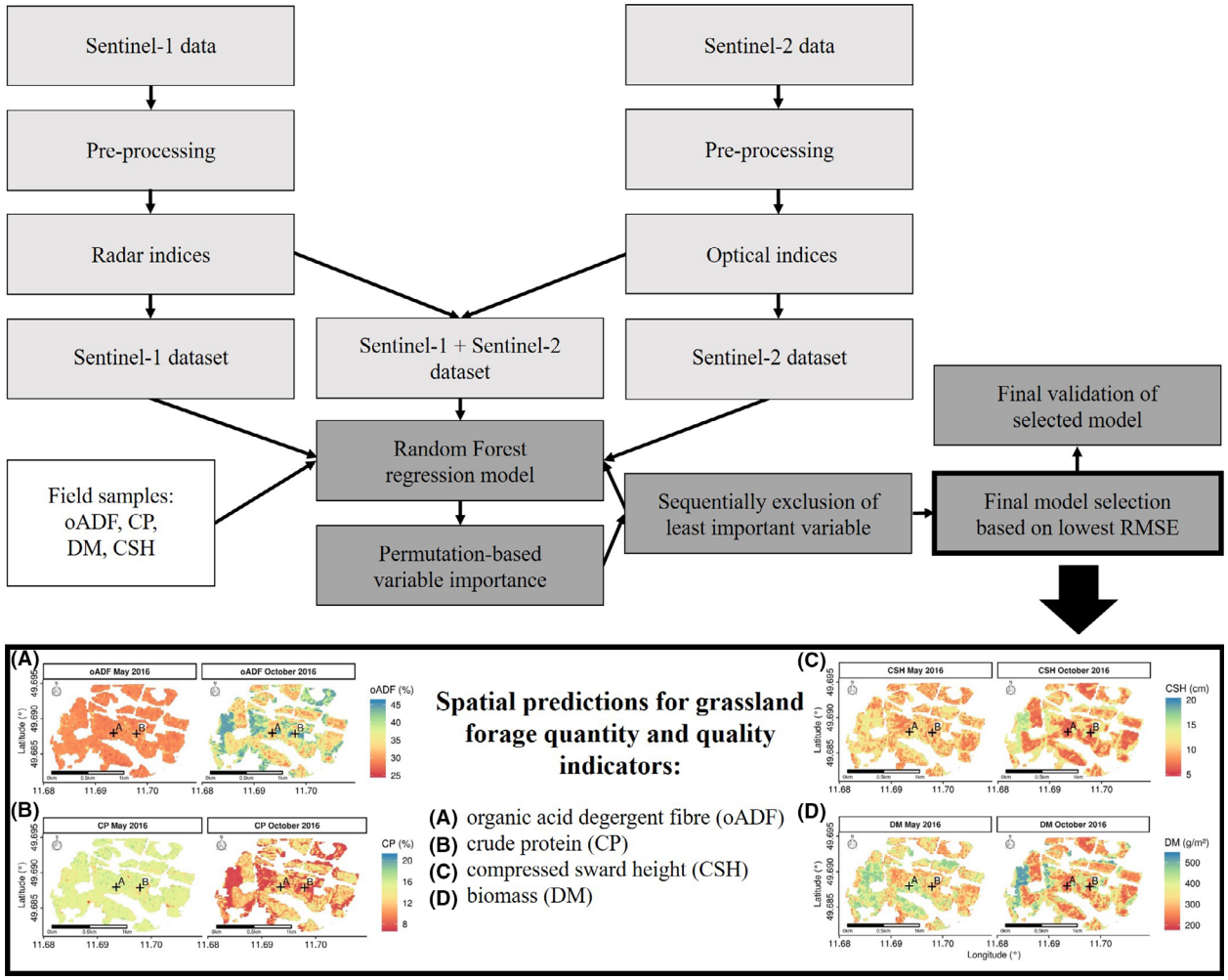

Figure 4. Schematic illustration of the processing steps.

Table 2. Spectral and spatial specifications of the Sentinel-2 constellation

Band	Band name	Spatial resolution (m)	Wavelength centre (nm)	Spectral width (nm)
1	Coastal aerosol	60	443	20
2	Blue	10	490	65
3	Green	10	560	35
4	Red	10	665	30
5	Red-edge-1	20	705	15
6	Red-edge-2	20	740	15
7	Red-edge-3	20	783	20
8	NIR	10	842	115
8A	Narrow NIR	20	865	20
9	Water vapour	60	945	20
10	SWIR-cirrus	60	1375	30
11	SWIR-1	20	1610	90
12	SWIR-2	20	2190	180

NIR, near-infrared; SWIR, short-wave infrared.

Calculation of indices

Vegetation indices (VIs) are established as a suitable tool for the analysis of plant dynamics and ecosystem monitoring by multispectral satellite remote sensing (Pettorelli et al. 2005), including the chemical composition (Clevers and Gitelson 2013; Frampton et al. 2013; Tong and He 2017; Loozen et al. 2019) and quantity (Silleos et al. 2006; Ramoelo et al. 2015b; Schweiger et al. 2015) of grassland biomass. Most VIs are relatively easy to compute and are able to reduce variability introduced by site-specific conditions, such as bare soil, illumination angle or the atmosphere. Hence, 77 multispectral-based vegetation indices were included, commonly found in the literature.

In addition, five biophysical products (L2B) were derived using the biophysical processor in SNAP. These L2B products included leaf area index, fraction of

absorbed photosynthetically active radiation, cover fraction, canopy water content and canopy chlorophyll content. L2B variables were included in order to evaluate a potential information gain related to model-based biophysical variables, as for example shown for the leaf area index and crop production (Lambert et al. 2018). Moreover, six radar indices, such as simple ratios were added to the analyses. In total, 102 predictor variables were available for the grassland forage quantity and quality random forest regression models, including 10 multispectral bands, 77 vegetation indices, 5 L2B products, 4 radar bands from different orbits and 6 radar indices. All included predictor variables can be found in Tables S1−S3 of the supplementary material. To evaluate a potential benefit of combining optical Sentinel-2 with radar Sentinel-1 data, three different predictor variable sets were composed out of the 102 available predictor variables: (i) predictor variables originating from Sentinel-2 data only (S2), (ii) Sentinel-1 only (S1) and (iii) a combination of both (S2 + S1).

Statistical analysis

The random forest regression algorithm was used to assess the relationships between grassland forage quantity and quality and remote sensing derived datasets. In a first step, the three different predictor variable sets were applied to the RF algorithm in order to compare the change in model performance depending on the selected input variables. These models used either predictor variables originating from (i) Sentinel-2 data only, (ii) Sentinel-1 only and (iii) a combination of both. All analyses were initially performed with a full predictor dataset respectively. The model performance was estimated as the root mean square error (RMSE) using a 10-fold cross-validation:

$$\mathrm{RMSE} = \sqrt{\frac{\sum_{n=1}^{n} (Yi - \hat{Y}i)^2}{n}} \quad (1)$$

where Yi is the measured value, $\hat{Y}i$ the predicted value of cases i and n equals the number of observations. The 10-fold cross-validation partitions the dataset randomly into 10-1 folds for training and uses the remaining fold for testing the model. In this context, $\mathrm{RMSE}_{\mathrm{testing}}$ refers to the RMSE when the trained model is applied to the testing data and $\mathrm{RMSE}_{\mathrm{training}}$ to the RMSE when the trained model is applied to the data used for training. Both measures in comparison can provide an indication of how strongly the RF adapts to the training data and how stable the predictions on validation data are. In addition, predictor variable importance was estimated using a permutation approach (Ruß and Brenning 2010; Brenning 2012). Because the internal importance measure of the RF was shown to be biased (Strobl et al. 2007), and the conditional RF is very computationally intensive (Nicodemus et al. 2010), the applied permutation-based variable selection can be seen as an appropriate strategy. The least important variable was determined by excluding one variable at a time from the model and calculating the mean decrease in RMSE after 100 permutations and 100 repetitions. The variable whose exclusion caused the smallest increase in RMSE was permanently removed from the respective model. Based on an a priori decision, this process was repeated until only two variables were left in the final model. From this pool of results, the $\mathrm{RMSE}_{\mathrm{min}}$ and $\mathrm{RMSE}_{\mathrm{max}}$ indicated the best (optimized) and worst performing model respectively.

In a second step, an optimized predictor variable combination for each response variable (oADF, CP, CSH and DM) was selected based on $\mathrm{RMSE}_{\mathrm{min}}$ from all calculated models. These respective optimized final models were additionally validated using a 10-fold cross-validation procedure with 1000 repetitions. The calculation of variable importance for each optimum model was estimated with 1000 permutations per predictor variable. In order to evaluate how the final model performed on the training and testing data, both $\mathrm{RMSE}_{\mathrm{training}}$ and $\mathrm{RMSE}_{\mathrm{testing}}$ were derived for the respective final model. The corresponding standard deviation (e.g. $\mathrm{RMSE}_{\mathrm{training\ sd}}$) values provide a measure of model robustness with regard to the input data. All RF models were built using default settings. The number of variables randomly sampled as candidates at each split (mtry) were set to the number of input variables divided by three, constructed with 500 trees (num.trees) (Belgiu and Drăguţ 2016).

Finally, the spatial distribution of oADF, CP, CSH and DM was predicted using the best variable combination. All final maps were averaged over 100 predictions.

All analyses were carried out within the R statistical programming environment (R Core Team, 2018) using the packages *ranger* for RF regression (Wright and Ziegler 2015), *mlr* (Bischl et al. 2016) for cross-validation and permutation, and *raster* (Hijmans 2017) for the spatial predictions.

Results

Selection of predictor dataset and validation

A relatively weak performance was observed for models with Sentinel-1 data only, compared to models where Sentinel-2 data were included (Table 3). The lowest RMSE and highest R^2 for oADF, CP and CSH were reached using the combined Sentinel-1 and Sentinel-2 predictor dataset. For DM, the lowest RMSE was obtained by the Sentinel-2 only dataset, but the difference to the

Table 3. Performance of the three different predictor datasets estimated using random forest regression. Predictors were iteratively removed based on variable importance

	oADF (%)			CP (%)			CSH (cm)			DM (g/m²)		
	S1	S2	S1 + S2	S1	S2	S1 + S2	S1	S2	S1 + S2	S1	S2	S1 + S2
$RMSE_{mean}$	5.42	2.51	2.41	3.43	1.84	1.78	4.38	2.90	2.89	123.99	94.22	95.14
$RMSE_{max}$	5.51	2.71	2.70	3.52	2.13	2.1	4.55	3.44	3.44	127.75	111.24	111.44
$RMSE_{min}$	5.32	2.37	**2.29**	3.38	1.78	**1.70**	4.11	2.79	**2.76**	120.48	**90.63**	90.82
$RMSE_{sd}$	0.07	0.06	0.08	0.04	0.04	0.06	0.15	0.08	0.09	2.08	2.61	2.55
R^2 mean	−0.07	0.75	0.77	−0.09	0.68	0.70	0.00	0.56	0.56	−0.01	0.41	0.40
R^2 max	−0.02	0.78	**0.79**	−0.05	0.7	**0.73**	0.12	0.59	**0.60**	0.04	**0.45**	**0.45**
R^2 min	−0.01	0.71	0.71	−0.15	0.57	0.58	−0.08	0.36	0.36	−0.09	0.17	0.16
R^2 *sd*	0.03	0.01	0.01	0.03	0.02	0.02	0.06	0.03	0.03	0.04	0.03	0.03

The R^2 and RMSE testing values are means of 100 repetitions of a 10-fold cross-validation. The lowest RMSE and highest R^2 values are highlighted in bold (Abbreviations: oADF, organic acid detergent fibre concentration; CP, crude protein concentration; CSH, compressed sward height; DM, standing biomass dry matter weight; S1, Sentinel-1 predictor dataset; S2, Sentinel-2 predictor dataset; S1 + S2, combined Sentinel-1 and Sentinel-2 predictor dataset).

combined Sentinel-1 and Sentinel-2 predictor dataset was marginal. Therefore, all subsequent analyses were conducted with the combined Sentinel-1 and Sentinel-2 dataset.

The validation results after recursively removing predictor variables from the combined Sentinel-1 and Sentinel-2 dataset are illustrated in Figure 5. Starting with a full set of 102 variables, removing predictor variables initially increased the R^2 value. After reaching a maximum, the R^2 rapidly decreased for oADF, CP, CSH and DM. A reverse behaviour was observed for the normalized RMSE. For visualization purposes, the normalization is expressed between zero and one according to the observed $RMSE_{min}$ and $RMSE_{max}$. The models with the lowest RMSE contained 8−15 predictor variables (Table 4).

The high R^2 testing values indicated a good match between observed and predicted oADF and CP concentrations. This was supported by relatively low $RMSE_{testing}$ values in comparison to the range of oADF and CP concentrations measured in the field (Table 4). The small R^2 and $RMSE_{testing\ sd}$ values after 1000 repetitions further supported good model performances. For CSH and DM,

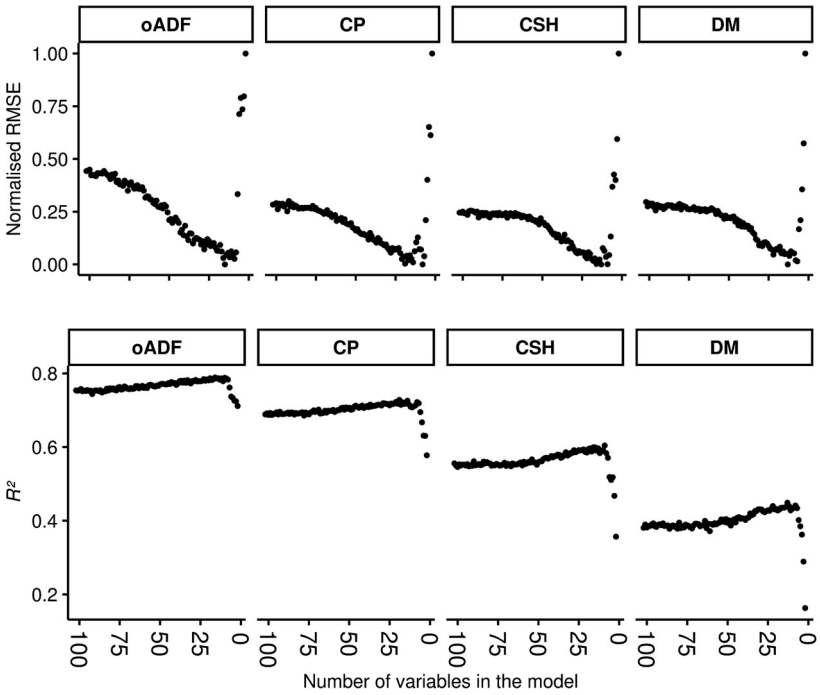

Figure 5. Changes in R^2 and normalised RMSE depending on the number of predictor variables remaining in the random forest regression model as variables are iteratively removed from the combined Sentinel-1 and Sentinel-2 predictor dataset. Abbreviations see Table 3.

Table 4. Statistics reporting the comparison of the selected best models

	oADF (%)	CP (%)	CSH (cm)	DM (g/m²)
Min observed	23.37	5.91	2.93	117.57
Max observed	47.97	21.33	25.55	630.07
$RMSE_{testing}$	2.29	1.70	2.77	90.84
$RMSE_{testing\ sd}$	0.42	0.35	0.60	17.63
$RMSE_{training}$	0.99	0.75	1.20	39.18
$RMSE_{training\ sd}$	0.02	0.02	0.03	0.95
R^2 testing	0.79	0.72	0.60	0.45
R^2 testing *sd*	0.13	0.15	0.17	0.23
R^2 training	0.97	0.96	0.94	0.91
R^2 training *sd*	<0.01	<0.01	<0.01	<0.01
Number of variables	15	8	13	13
Number of radar variables	2	1	2	0

The R^2 and RMSE values are means of 1000 repetitions of a 10-fold cross-validation using random forest regression. Abbreviations see Table 3.

lower R^2 testing values were observed compared to oADF and CP. The estimated RMSE values were moderately higher, considering the respective observed range of the data. For both CSH and DM, 13 predictor variables remained in the final model.

Variable importance

Permutation-based variable importance was used to identify important predictor variables for oADF, CP, CSH and DM from the optimized combined Sentinel-1 and Sentinel-2 dataset (see Fig. 6). For oADF and CP, the most important variable was the simple ratio between the narrow near-infrared (B8A) and the red-edge-3 (B7) band. Excluding this simple ratio from the model decreased the performance in terms of R^2 by 0.10 for oADF and 0.18 for CP. A similar simple ratio, narrow near-infrared divided by red-edge-2 (B6), contributed substantially to the model performance of CSH and DM. For DM, R^2 decreased by 0.22 when this particular simple ratio was excluded from the model. For CSH, the simple ratio between the short-wave infrared-2 (B12) and the red (B4) band was found to be the most relevant variable. Single multispectral bands were in the optimized predictor dataset for oADF, CSH and DM, but their removal did not decrease R^2 by more than 0.06. The Soil Adjusted

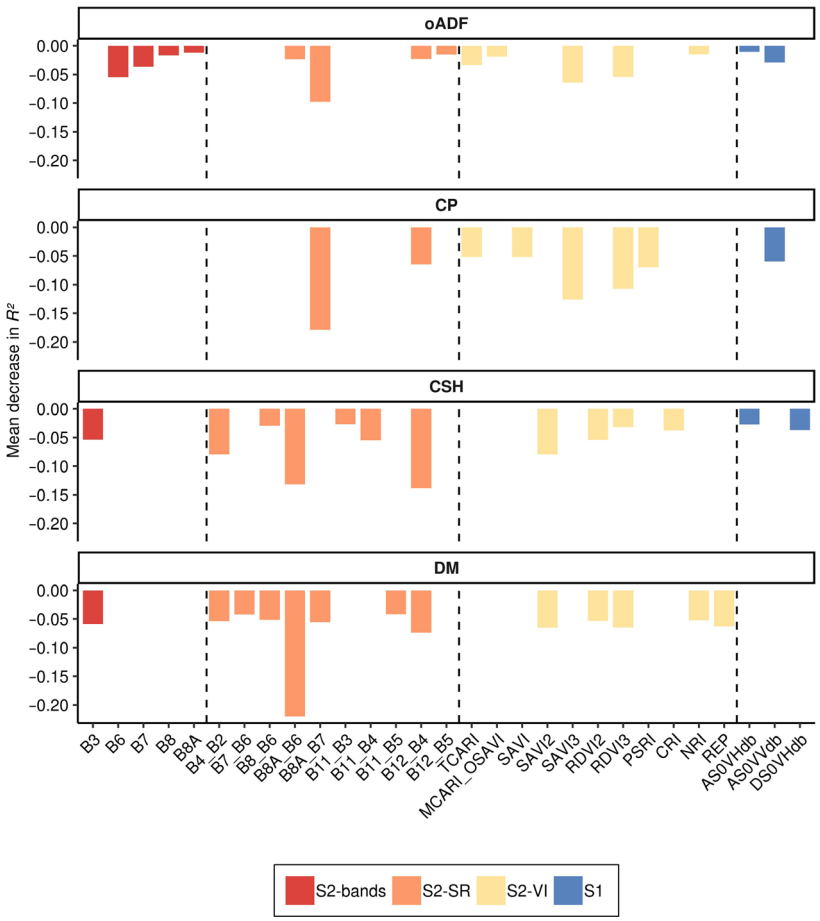

Figure 6. Permutation-based variable importance derived as an decrease in R^2 caused by excluding one variable and keeping the rest in the model. Explanations to the respective *x*-axis labels can be found in the supplementary material (Tables S1–S3). B = band (Table 2), underscore = divided by. Abbreviations see Table 3.

Vegetation Index (SAVI) and its extensions, which use different red-edge bands instead of the red band, were important for oADF, CP, CSH and DM. Other vegetation indices contributed to the model performances to smaller extents. For CP, vegetation indices were more important than for oADF, CSH and DM. Sentinel-1 variables were only selected for oADF, CP and CSH models. The general contribution of SAR variables was low compared to simple ratios or vegetation indices. No L2B variable was selected by the variable optimization process.

Spatial prediction

Figure 7 displays the spatial predictions for oADF, CP, CSH and DM derived from the optimized predictor variables by applying the respective RF model. For illustration purposes, the figures and following descriptions are presented for the area surrounding the two sample locations A and B of Figure 1. Only the results for May and October 2016 are presented; spatial predictions for further sampling dates can be found in Figures S1–S3 in the supplementary material.

A relatively even distribution of oADF concentrations was observed for May 2016 (Fig. 7a). In October 2016, the spatial distribution of concentrations was more differentiated, especially at the edges of the masked non-grassland areas. The mean predicted oADF concentration was about 29.3% (sd = 0.97) for May and about 36.6% (sd = 4.52) for October 2016, which corresponds to the observed concentrations in Figure 3.

Similar to oADF, a relatively even distribution of CP concentrations was observed for May 2016 (Fig. 7b). The mean CP concentration in May 2016 was about 15.1% (sd = 0.98). For October 2016, the spatial distribution of CP showed a distinct differentiation in areas with CP concentrations either above or below approximately 8%, with a mean predicted CP concentration of 10.8% (sd = 2.54).

For May 2016, a mean CSH of 10.3 cm (sd = 1.84) and for October a mean CSH of 9.9 cm (sd = 2.64) were predicted. Similar to the predictions of CP, CSH showed a spatial differentiation, with values either below or above 10 cm (Fig. 7c). A corresponding distinction was present for the DM predictions. A mean DM of 355.0 g/m² (sd = 67.0) in May and 329.9 g/m² (sd = 84.18) in October was predicted. In general, a more even spatial distribution of oADF and CP concentrations in May and a more pronounced differentiation in October 2016 was observed. This was similar for CSH and DM, but with a higher degree of variance in May. Areas with high CP and low oADF concentrations in October 2016 were related to areas with low CSH and DM values, and vice versa. A similar but less pronounced pattern between the predicted vegetation characteristics was observed for the spatial predictions in May.

Discussion

This study shows that semi-natural grassland forage quality indicators can be mapped with high accuracy, as R^2 values of the regression models ranged from 0.72 (sd = 0.15) for CP to 0.79 (sd = 0.13) for oADF. For the grassland forage quantity indicators, lower R^2 values were obtained (R^2 = 0.60, sd = 0.17 for CSH and R^2 = 0.45, sd = 0.23 for DM). When analysed separately, Sentinel-1 data had a low performance for all considered indicators. When Sentinel-1 data were added to Sentinel-2 data, the RF model performance increased only marginally. In particular, the max R^2 values of all models considered in Table 3 were only higher by 0.025 for CP and about 0.012 higher for oADF and CSH for the combination of both data sources. For DM, the difference was negligible.

Sentinel-1 data for grassland forage quantity and quality prediction

Despite the generally low contribution of Sentinel-1 data to the model performance, between one and two radar variables were among the most important variables for the prediction of oADF, CP and CSH (Fig. 6). The small contribution of Sentinel-1 data to the final models might be attributed to the wavelength (5.6 cm) of the C-band sensor. Even though the amount of studies concerned with the estimation of biophysical parameters for semi-natural grasslands is limited, Zalite et al. (2016) demonstrated the potential of X-band data with a wavelength of about 3 cm to map biophysical parameters on agricultural grassland. For this purpose, HH-polarized COSMO-SkyMed 1-day repeat-pass SAR pairs were used to inversely relate temporal interferometric coherence to vegetation height and fresh above-ground biomass. In addition, Ali et al. (2017a) showed that TerraSAR-X interferometric coherence data can be used successfully to predict agricultural grassland height (R^2 = 0.55) and biomass (R^2 = 0.75) at the paddock scale. Thus, further research is required to investigate the potential contribution of Sentinel-1 coherence data to predict semi-natural grassland forage quality and quantity indicators.

Optimization of the predictor dataset and important variables

As the applied predictor variable optimization, that is, repeated exclusion of the least important variable based on permutation, increased the predictive power of the

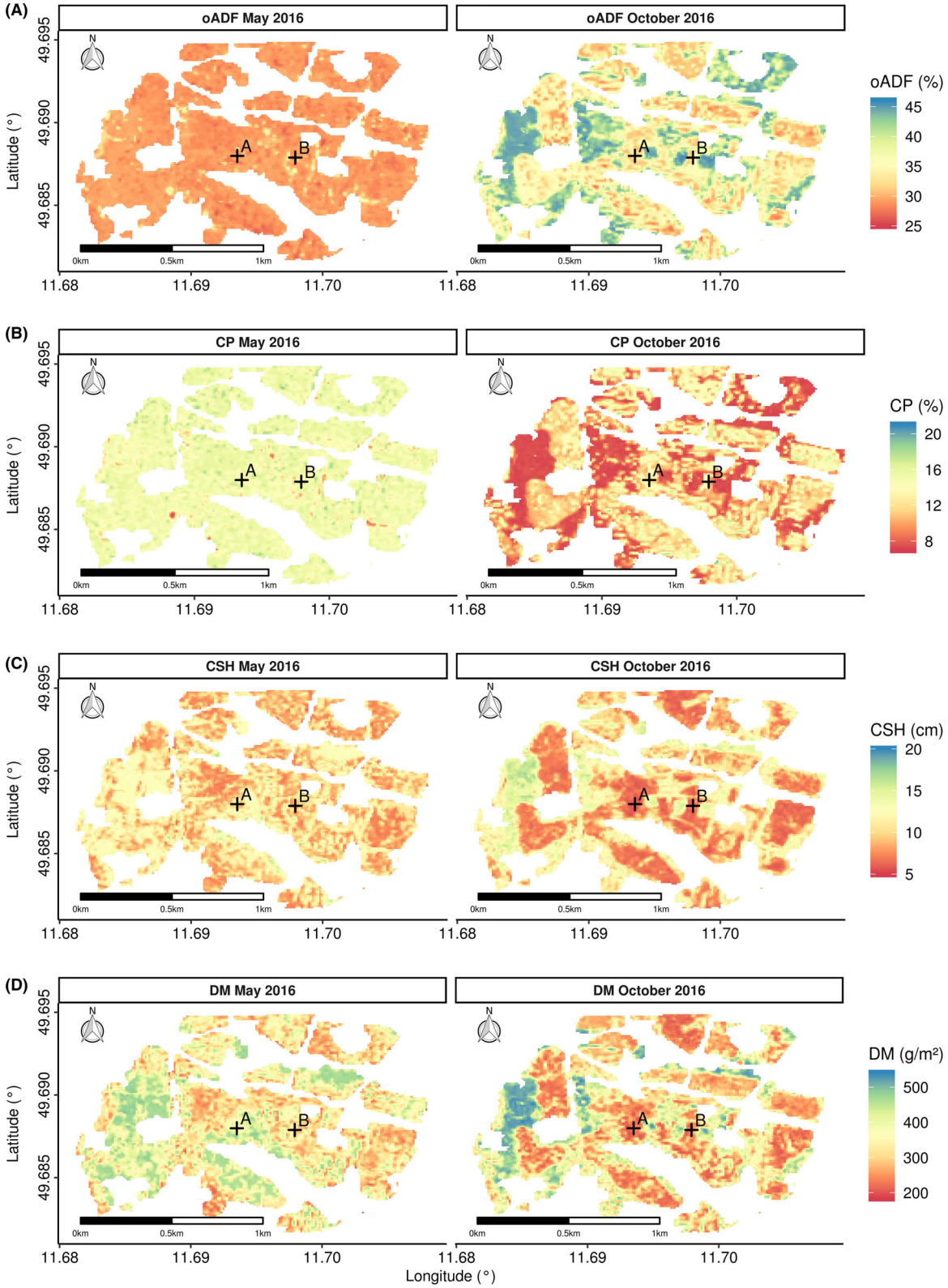

Figure 7. Spatial predictions of oADF, CP, CSH and DM for May and October 2016 using random forest regression, averaged over 100 repetitions. The illustrations are presented for the area surrounding the two sampling locations A and B of Figure 1. Abbreviations see Table 3.

random forest models in all cases, a careful selection of variables regarding the biophysical parameter of interest is recommended.

This study confirmed the importance of the red-edge region to predict biophysical parameters, previously found by several other studies (Delegido et al. 2011; Duan et al. 2012; Ramoelo et al. 2012, 2015b; Verrelst et al. 2012; Clevers and Gitelson 2013; Frampton et al. 2013; Tong and He 2017). The red-edge region describes the spectral feature between the red absorption maximum and a reflectance peak in the near-infrared, which can be linked to the chemical composition of vegetation and vegetation biomass (Clevers and Gitelson 2013; Frampton et al. 2013). However, Punalekar et al. (2018) found that the 10 m bands (i.e. without red-edge bands) from in situ hyperspectral data resampled to Sentinel-2A were sufficient to estimate LAI using a radiative transfer model (PROSAIL) on agricultural grassland. The LAI in turn can be related to vegetation biomass (e.g. Friedl et al. (1994) and Dusseux et al. (2014)). With regard to the low performance of the DM and CSH models, the relevance of the red-edge region in this context is difficult to disentangle.

No L2B products were selected by the variable optimization process for all quantity and quality indicators. The derived L2B products were modelled using the SNAP biophysical processor. As they were based on multispectral bands of the Sentinel-2 data, this may have increased the complexity of the model with a low degree of information gain. With regard to the computationally demanding SNAP biophysical processor and the high variable importance of simple ratio-based indices, spectral indices may be sufficient to map semi-natural grassland quantity and quality indicators.

As illustrated in Figure 3, the negative relationship between CP and vegetation quantity indicators (CSH and DM) was very pronounced until mowing in July. This was similar to the relationship between CP and oADF, that is, a high concentration of CP was related to a lower concentration of oADF and vice versa. The reflectance in the near-infrared-part can be related to leaf and canopy structure, while the red-edge region is related to chlorophyll concentration (Sims and Gamon 2002; Tong and He 2017). As the chlorophyll concentration is related to the crude protein concentration, the high importance of simple ratios between the narrow near-infrared band 8A and one of the red-edge bands can be linked to the integration of near-infrared and red-edge reflectance in one variable, that is, a simple ratio (Fig. 6).

The result of the variable optimization depends on the pool of variables selected by the user. Thus, the variables selected by the optimization process must be considered as only one possible solution to model the relationship of semi-natural grassland forage quantity and quality. However, as the predictive power increased until the optimal number and combination of variables were reached and decreased thereafter, the variable selection process in the context of random forest machine learning must be seen as an important and reasonable processing step (Gregorutti et al. 2017).

Sampling plot size

As the sampling data collection strategy of Riesch et al. (2019) was not designed to be applied to satellite remote sensing data, the plot size of 15 × 15 m may have introduced some degree of uncertainty with regard to the geolocation error of the used Sentinel-1 and Sentinel-2 data. However, the sampled plots were embedded in a larger treatment area of the same management. Thus, potential uncertainties introduced by the geolocation error can be considered as low. In order to reduce the geolocation error effect, future studies should be more careful when the plot size is selected. For this, the equation by Justice and Townshend (1981) can be used to calculate the required plot size,

$$S = P(1 + 2L) \tag{2}$$

where S equals the side length of the sampling plot, P is the pixel size of the used sensor in metres and L is the sensor specific geolocation error in pixels. In addition, a buffer distance to environmentally different areas can further minimize side effects (Zandler et al. 2015).

Remote sensing for the conservation of semi-natural grassland

For pasture management purposes, remote sensing has been proven to be a valuable tool to predict grassland forage mass and quality indicators (Ali et al. 2016; Wachendorf et al. 2017). Such information can be of high importance for farmers, for example, for rotational grazing systems, as well as for conservation (e.g. Punalekar et al. (2018)). Marginal areas, however, are often characterized by a heterogeneous land cover composition. In the special case of an active military training area, access restrictions challenge the management and conservation of open habitats, such as semi-natural grasslands (Riesch et al. 2019). Under such landscape conditions, the potential of wild herbivores as a management and conservation option has recently been acknowledged (Pausas and Bond 2018; Schulze et al. 2018). For the GTA, Riesch et al. (2019) showed that red deer can contribute significantly to the conservation of semi-natural grassland ecosystems. In particular, it was shown that forage removal was enhanced in

mown grassland, related to an increased productivity and forage quality (Riesch et al. 2019). The present study provides evidence that for semi-natural grassland ecosystems forage mass and quality indicators can be successfully predicted using freely available Sentinel data. This remote sensing-based approach has the potential to become a helpful tool in future wildlife and conservation management. Remote sensing derived information about forage conditions allows for almost real-time decisions by managers concerning fencing, supplementary feeding and provide information to assess the current forage supply. In addition, dense time series of remote sensing data can further facilitate the evaluation of grazing and browsing behaviours covering different phenological phases (Dupke et al. 2017). Thus, the change in biophysical vegetation properties can be related to the spatial-temporal distribution of herbivores and may allow for an evaluation of the sustainability of the current grazing system. This concept is generally applicable to both wildlife and domestic life stock, though different management tools need to be utilized to steer life stock versus wildlife. For example, the spatial-temporal distribution of life stock is often controlled directly by guiding animals into certain areas, via fences or herding dogs. With free-roaming wildlife, fences can often only be applied locally, but the spatial-temporal behaviour of wildlife can be influenced across the landscape by habitat management (e.g. mowing, burning; Riesch et al. 2019) and by hunting (Cromsigt et al. 2013). Thus, for both life stock and wildlife, managers can use the estimated foraging conditions to identify those areas where, at any given time, grazing by herbivores is most desirable, and where overgrazing needs to be avoided. The most important advantage of using remote sensing within such a target-oriented grazing management is the fact that remote sensing can provide the necessary foraging data across large areas and for multiple times, without the need to repeatedly conduct cost- and labour-intensive field work which also leads to disturbances in the case of wildlife.

Conclusion

The present study has evaluated the possibilities of combining Sentinel-1 and Sentinel-2 data for estimating semi-natural grassland quantity and quality. Predictor variables derived from the Sentinel-2 sensors were sufficient to accurately predict organic acid detergent fibre concentration and crude protein concentration from field observations. For compressed sward height and standing biomass dry weight the results were less accurate. A repeated reduction of the predictor variable set was implemented, guided by a permutation-based variable importance measure. Thus, a subset of important variables was identified. The simple ratios between the narrow near-infrared and red-edge region were found to be particularly important. As the spatial distribution and the activities of large herbivores are affected by the availability and quality of potential forage areas, this may support the future conservation of semi-natural grassland ecosystems grazed by livestock species or wildlife.

Acknowledgments

The project was supported by funds of German government's Special Purpose Fund held at Landwirtschaftliche Rentenbank (28 RZ 7007). We thank the Federal Forests Division (Bundesforst) of the German Institute for Federal Real Estate (Bundesanstalt für Immobilienaufgaben) and the Institut für Wildbiologie Göttingen und Dresden e.V. for close cooperation and support. We acknowledge support by the Open Access Publication Funds of the Göttingen University.

Conflict of Interest

The authors declare no conflict of interest.

Funding Information

The project was supported by funds of German government's Special Purpose Fund held at Landwirtschaftliche Rentenbank (28 RZ 7007).

References

Adesogan, A. T., D. I. Givens, and E. Owen. 2000. Measuring chemical composition and nutritive value in forages. Pp. 263–278 *in* L t' Mannetje and R. M. Jones, eds. *Field and laboratory methods for grassland and animal production research*. CABI Publishing, Warwickshire.

Ali, I., F. Cawkwell, E. Dwyer, B. Barrett, and S. Green. 2016. Satellite remote sensing of grasslands: from observation to management-a review. *J. Plant Ecol.* **9**, 649–671

Ali, I., B. Barrett, F. Cawkwell, S. Green, E. Dwyer, and M. Neumann. 2017a. Application of repeat-pass TerraSAR-X staring spotlight interferometric coherence to monitor pasture biophysical parameters: limitations and sensitivity analysis. *IEEE J. Sel. Top. Appl. Earth Obs. Remote Sens.* **10**, 3225–3231.

Ali, I., F. Cawkwell, E. Dwyer, and S. Green. 2017b. Modeling managed grassland biomass estimation by using multitemporal remote sensing data—a machine learning approach. *IEEE J. Sel. Top. Appl. Earth Obs. Remote Sens.* **10**, 3254–3264.

Barrett, B., I. Nitze, S. Green, and F. Cawkwell. 2014. Assessment of multi-temporal, multi-sensor radar and ancillary spatial data for grasslands monitoring in Ireland using machine learning approaches. *Remote Sens. Environ.* **152**, 109–124.

Beckschäfer, P., L. Fehrmann, R. D. Harrison, J. Xu, and C. Kleinn. 2014. Mapping Leaf Area Index in subtropical upland ecosystems using RapidEye imagery and the randomForest algorithm. *IForest* **7**, 1.

Belgiu, M., and L. Drăguţ. 2016. Random forest in remote sensing: a review of applications and future directions. *ISPRS J. Photogramm. Remote Sens.* **114**, 24–31.

Bischl, B., M. Lang, L. Kotthoff, J. Schiffner, J. Richter, E. Studerus, et al. 2016. mlr: machine learning in R. *J. Mach. Learn. Res.* **17**, 1–5.

Borer, E. T., E. W. Seabloom, D. S. Gruner, W. S. Harpole, H. Hillebrand, E. M. Lind, et al. 2014. Herbivores and nutrients control grassland plant diversity via light limitation. *Nature* **508**, 517.

Breiman, L. 2001. Random forests. *Mach. Learn* **45**, 5–32.

Brenning, A. 2012. Spatial cross-validation and bootstrap for the assessment of prediction rules in remote sensing: the R package sperrorest. Pp. 5372–5375 in Geoscience and Remote Sensing Symposium (IGARSS), 2012 IEEE International. IEEE.

Brodu, N. 2017. Super-resolving multiresolution images with band-independent geometry of multispectral pixels. *IEEE Trans. Geosci. Remote Sens.* **55**, 4610–4617.

Bunzel-Drüke, M. 2008. "Wilde Weiden": Praxisleitfaden für Ganzjahresbeweidung in Naturschutz und Landschaftsentwicklung. Arbeitsgem. Biologischer Umweltschutz im Kreis Soest eV (ABU).

Catchpole, W. R., and C. J. Wheeler. 1992. Estimating plant biomass: a review of techniques. *Aust. J. Ecol.* **17**, 121–131.

Catorci, A., F. M. Tardella, K. Piermarteri, R. Pennesi, L. Malatesta, M. Corazza, et al. 2016. Effect of red deer grazing on alpine hay meadows: biodiversity and management implications. *Appl. Ecol. Environ. Res.* **14**, 301–318.

Cho, M. A., and A. K. Skidmore. 2006. A new technique for extracting the red edge position from hyperspectral data: the Linear Extrapolation Method. *Remote Sens. Environ.* **101**, 181–193.

Clevers, J. G., and A. A. Gitelson. 2013. Remote estimation of crop and grass chlorophyll and nitrogen content using red-edge bands on Sentinel-2 and-3. *Int. J. Appl. Earth Obs.* **23**, 344–351.

Clevers, J., L. Kooistra, and M. Van Den Brande. 2017. Using Sentinel-2 data for retrieving LAI and leaf and canopy chlorophyll content of a potato crop. *Remote Sens.* **9**, 405.

Correll, O., J. Isselstein, and V. Pavlu. 2003. Studying spatial and temporal dynamics of sward structure at low stocking densities: the use of an extended rising-plate-meter method. *Grass Forage Sci.* **58**, 450–454.

Cortes, C., and V. Vapnik. 1995. Support-vector networks. *Mach. Learn* **20**, 273–297.

Cromsigt, J. P., D. P. Kuijper, M. Adam, R. L. Beschta, M. Churski, A. Eycott, et al. 2013. Hunting for fear: innovating management of human–wildlife conflicts. *J. Appl. Ecol.* **50**, 544–549.

Dangal, S. R., H. Tian, C. Lu, S. Pan, N. Pederson, and A. Hessl. 2016. Synergistic effects of climate change and grazing on net primary production of Mongolian grasslands. *Ecosphere* **7**, e01274.

Delegido, J., J. Verrelst, L. Alonso, and J. Moreno. 2011. Evaluation of sentinel-2 red-edge bands for empirical estimation of green LAI and chlorophyll content. *Sensors* **11**, 7063–7081.

Delloye, C., M. Weiss, and P. Defourny. 2018. Retrieval of the canopy chlorophyll content from Sentinel-2 spectral bands to estimate nitrogen uptake in intensive winter wheat cropping systems. *Remote Sens. Environ.* **216**, 245–261.

Dengler, J., M. Janišová, P. Török, and C. Wellstein. 2014. Biodiversity of Palaearctic grasslands: a synthesis. *Agric. Ecosyst. Environ.* **182**, 1–14.

Drusch, M., U. Del Bello, S. Carlier, O. Colin, V. Fernandez, F. Gascon, et al. 2012. Sentinel-2: ESA's optical high-resolution mission for GMES operational services. *Remote Sens. Environ.* **120**, 25–36.

Duan, M., Q. Gao, Y. Wan, Y. Li, Y. Guo, Z. Ganzhu, et al. 2012. Biomass estimation of alpine grasslands under different grazing intensities using spectral vegetation indices. *Can. J. Remote. Sens.* **37**, 413–421.

Dupke, C., C. Bonenfant, B. Reineking, R. Hable, T. Zeppenfeld, M. Ewald, et al. 2017. Habitat selection by a large herbivore at multiple spatial and temporal scales is primarily governed by food resources. *Ecography* **40**, 1014–1027.

Dusseux, P., T. Corpetti, L. Hubert-Moy, and S. Corgne. 2014. Combined use of multi-temporal optical and radar satellite images for grassland monitoring. *Remote Sens.* **6**, 6163–6182.

ESA. 2016a. User Guides - Sentinel-1 SAR - Sentinel Online [WWW Document]. https://earth.esa.int/web/sentinel/user-guides/sentinel-1-sar (accessed 7.23.18).

ESA. 2016b. SNAP. ESA Sentinel Application Platform.

Felton, A. M., H. K. Wam, C. Stolter, K. M. Mathisen, and M. Wallgren. 2018. The complexity of interacting nutritional drivers behind food selection, a review of northern cervids. *Ecosphere* **9**, e02230.

Fløjgaard, C., M. De Barba, P. Taberlet, and R. Ejrnæs. 2017. Body condition, diet and ecosystem function of red deer (*Cervus elaphus*) in a fenced nature reserve. *Glob. Ecol. Conserv.* **11**, 312–323.

Frampton, W. J., J. Dash, G. Watmough, and E. J. Milton. 2013. Evaluating the capabilities of Sentinel-2 for quantitative estimation of biophysical variables in vegetation. *ISPRS J. Photogramm. Remote Sens.* **82**, 83–92.

Friedl, M. A., D. S. Schimel, J. Michaelsen, F. W. Davis, and H. Walker. 1994. Estimating grassland biomass and leaf area index using ground and satellite data. *Int. J. Remote Sens.* **15**, 1401–1420.

Gibson, D. J. 2009. *Grasses and grassland ecology*. Oxford University Press, Oxford, UK.

Gregorutti, B., B. Michel, and P. Saint-Pierre. 2017. Correlation and variable importance in random forests. *Stat. Comput.* **27**, 659–678.

Haykin, S. 1994. *Neural networks: a comprehensive foundation*. Prentice Hall PTR, Upper Saddle River, NJ.

Hijmans, R. J. 2017. raster: geographic data analysis and modeling. R Package Version 26-7.

Huete, A. R., K. Didan, T. Miura, E. P. Rodriguez, X. Gao, and L. G. Ferreira. 2002. Overview of the radiometric and biophysical performance of the MODIS vegetation indices. *Remote Sens. Environ.* **83**, 195–213.

Isselstein, J. 2018. Protecting biodiversity in grasslands. Pp. 1–2 *in* A. Marshall, R. Collins, ed. *Improving grassland and pasture management in temperate agriculture*. Chapter 16, Burleigh Dodds Science Publishing, Cambridge, UK. ISBN: 978 1 78676 200 9; www.bdspublishing.com.

Isselstein, J., B. Jeangros, and V. Pavlu. 2005. Agronomic aspects of biodiversity targeted management of temperate grasslands in Europe–a review. *Agron. Res.* **3**, 139–151.

John, R., J. Chen, V. Giannico, H. Park, J. Xiao, G. Shirkey, et al. 2018. Grassland canopy cover and aboveground biomass in Mongolia and Inner Mongolia: spatiotemporal estimates and controlling factors. *Remote Sens. Environ.* **213**, 34–48.

Justice, C. O., and J. G. Townshend. 1981. Integrating ground data with remote sensing. Pp. 38–58 *in* J. G. Townshend, ed. *Terrain analysis and remote sensing*. Allen and Unwin, London.

Kawamura, K., T. Akiyama, H. Yokota, M. Tsutsumi, T. Yasuda, O. Watanabe, et al. 2005. Monitoring of forage conditions with MODIS imagery in the Xilingol steppe, Inner Mongolia. *Int. J. Remote Sens.* **26**, 1423–1436.

Kokaly, R. F., G. P. Asner, S. V. Ollinger, M. E. Martin, and C. A. Wessman. 2009. Characterizing canopy biochemistry from imaging spectroscopy and its application to ecosystem studies. *Remote Sens. Environ.* **113**, S78–S91.

Lamarque, P., S. Lavorel, M. Mouchet, and F. Quétier. 2014. Plant trait-based models identify direct and indirect effects of climate change on bundles of grassland ecosystem services. *Proc. Natl. Acad. Sci.* **111**, 13751–13756.

Lambert, M.-J., P. C. S. Traoré, X. Blaes, P. Baret, and P. Defourny. 2018. Estimating smallholder crops production at village level from Sentinel-2 time series in Mali's cotton belt. *Remote Sens. Environ.* **216**, 647–657.

Loozen, Y., D. Karssenberg, S. M. de Jong, S. Wang, J. van Dijk, M. J. Wassen, et al. 2019. Exploring the use of vegetation indices to sense canopy nitrogen to phosphorous ratio in grasses. *Int. J. Appl. Earth Obs.* **75**, 1–14.

t'Mannetje, L. 2000. Measuring biomass of grassland vegetation. Pp. 151–178 *in* L't Mannetje and R. M. Jones, eds. *Field and laboratory methods for grassland and animal production research*. CABI Publishing, Wallingford, UK.

Mannetje, L., and R. M. Jones. 2000. *Field and laboratory methods for grassland and animal production research*. CABI Publishing, Wallingford, UK.

Marsett, R. C., J. Qi, P. Heilman, S. H. Biedenbender, M. C. Watson, S. Amer, et al. 2006. Remote sensing for grassland management in the arid southwest. *Rangel. Ecol. Manag.* **59**, 530–540.

Merkle, J. A., K. L. Monteith, E. O. Aikens, M. M. Hayes, K. R. Hersey, D. Middleton, et al. 2016. Large herbivores surf waves of green-up during spring. *Proc. R. Soc. B Biol. Sci.* **283**, 20160456. https://doi.org/10.1098/rspb.2016.0456.

Müller-Wilm, U., O. Devignot, and L. Pessiot. 2018. *Sen2Cor configuration and user manual*. ESA, France.

Mutanga, O., and L. Kumar. 2007. Estimating and mapping grass phosphorus concentration in an African savanna using hyperspectral image data. *Int. J. Remote Sens.* **28**, 4897–4911.

Mutanga, O., A. K. Skidmore, and H. H. T. Prins. 2004. Predicting in situ pasture quality in the Kruger National Park, South Africa, using continuum-removed absorption features. *Remote Sens. Environ.* **89**, 393–408.

Mutanga, O., E. Adam, and M. A. Cho. 2012. High density biomass estimation for wetland vegetation using WorldView-2 imagery and random forest regression algorithm. *Int. J. Appl. Earth Obs.* **18**, 399–406.

Nakagami, K., and S. Itano. 2014. Improving pooled calibration of a rising-plate meter for estimating herbage mass over a season in cool-season grass pasture. *Grass Forage Sci.* **69**, 717–723.

Nicodemus, K. K., J. D. Malley, C. Strobl, and A. Ziegler. 2010. The behaviour of random forest permutation-based variable importance measures under predictor correlation. *BMC Bioinformatics* **11**, 110.

Palmer, S. C., A. J. Hester, D. A. Elston, I. J. Gordon, and S. E. Hartley. 2003. The perils of having tasty neighbors: grazing impacts of large herbivores at vegetation boundaries. *Ecology* **84**, 2877–2890.

Pausas, J. G., and W. J. Bond. 2018. Humboldt and the reinvention of nature. *J. Ecol.* **84**, 2877–2890.

Peeters, A., G. Beaufoy, R. M. Canals, A. De Vliegher, C. Huyghe, J. Isselstein, et al. 2014. Grassland term definitions and classifications adapted to the diversity of European grassland-based systems. *Grassl. Sci. Europe* 743–750.

Pellissier, P. A., S. V. Ollinger, L. C. Lepine, M. W. Palace, and W. H. McDowell. 2015. Remote sensing of foliar nitrogen in cultivated grasslands of human dominated landscapes. *Remote Sens. Environ.* **167**, 88–97.

Perbandt, D., T. Fricke, and M. Wachendorf. 2010. Effects of changing simulated sky cover on hyperspectral reflectance measurements for dry matter yield and forage quality prediction. *Comput. Electron. Agr.* **73**, 230–239.

Pettorelli, N., J. O. Vik, A. Mysterud, J.-M. Gaillard, C. J. Tucker, and N. C. Stenseth. 2005. Using the satellite-derived NDVI to assess ecological responses to environmental change. *Trends Ecol. Evol.* **20**, 503–510.

Punalekar, S. M., A. Verhoef, T. L. Quaife, D. Humphries, L. Bermingham, and C. K. Reynolds. 2018. Application of Sentinel-2A data for pasture biomass monitoring using a

physically based radiative transfer model. *Remote Sens. Environ.* **218**, 207–220.

R Core Team. 2018. *R: a language and environment for statistical computing*. R Foundation for Statistical Computing, Vienna,Austria. https://www.R-project.org/

Ramoelo, A., and M. Cho. 2018. Explaining leaf nitrogen distribution in a semi-arid environment predicted on Sentinel-2 imagery using a field spectroscopy derived model. *Remote Sens.* **10**, 269.

Ramoelo, A., A. K. Skidmore, M. A. Cho, M. Schlerf, R. Mathieu, and I. M. A. Heitkönig. 2012. Regional estimation of savanna grass nitrogen using the red-edge band of the spaceborne RapidEye sensor. *Int. J. Appl. Earth Obs.* **19**, 151–162.

Ramoelo, A., M. Cho, R. Mathieu, and A. K. Skidmore. 2015a. Potential of Sentinel-2 spectral configuration to assess rangeland quality. *J. Appl. Remote Sens.* **9**, 094096.

Ramoelo, A., M. A. Cho, R. Mathieu, S. Madonsela, R. Van De Kerchove, Z. Kaszta, et al. 2015b. Monitoring grass nutrients and biomass as indicators of rangeland quality and quantity using random forest modelling and WorldView-2 data. *Int. J. Appl. Earth Obs.* **43**, 43–54.

Raynor, E. J., A. Joern, J. B. Nippert, and J. M. Briggs. 2016. Foraging decisions underlying restricted space use: effects of fire and forage maturation on large herbivore nutrient uptake. *Ecol. Evol.* **6**, 5843–5853. https://doi.org/10.1002/ece3.2304.

Riesch, F., H. G. Stroh, B. Tonn, and J. Isselstein. 2018. Soil pH and phosphorus drive species composition and richness in semi-natural heathlands and grasslands unaffected by twentieth-century agricultural intensification. *Plant Ecol. Divers* **11**, 239–253.

Riesch, F., B. Tonn, M. Meißner, N. Balkenhol, and J. Isselstein. 2019. Grazing by wild red deer: management options for the conservation of semi-natural open habitats. *J. Appl. Ecol.* **7**, 1802–1822. https://doi.org/10.1111/1365-2664.13396.

Rosenthal, G., J. Schrautzer, and C. Eichberg. 2012. Low-intensity grazing with domestic herbivores: a tool for maintaining and restoring plant diversity in temperate Europe. *Tuexenia*, 167–205.

Ruß, G., and A. Brenning. 2010. Spatial variable importance assessment for yield prediction in precision agriculture. *Adv. Intell. Data Anal. IX.* 184–195.

Sanderson, M. A., C. A. Rotz, S. W. Fultz, and E. B. Rayburn. 2001. Estimating forage mass with a commercial capacitance meter, rising plate meter, and pasture ruler. *Agron. J.* **93**, 1281–1286.

Schulze, K. A., G. Rosenthal, and A. Peringer. 2018. Intermediate foraging large herbivores maintain semi-open habitats in wilderness landscape simulations. *Ecol. Model.* **379**, 10–21.

Schweiger, A. K., A. C. Risch, A. Damm, M. Kneubühler, R. Haller, M. E. Schaepman, et al. 2015. Using imaging spectroscopy to predict above-ground plant biomass in alpine grasslands grazed by large ungulates. *J. Veg. Sci.* **26**, 175–190.

Scurlock, J. M. O., and D. O. Hall. 1998. The global carbon sink: a grassland perspective. *Glob. Change Biol.* **4**, 229–233.

Si, Y., M. Schlerf, R. Zurita-Milla, A. Skidmore, and T. Wang. 2012. Mapping spatio-temporal variation of grassland quantity and quality using MERIS data and the PROSAIL model. *Remote Sens. Environ.* **121**, 415–425.

Silleos, N. G., T. K. Alexandridis, I. Z. Gitas, and K. Perakis. 2006. Vegetation indices: advances made in biomass estimation and vegetation monitoring in the last 30 years. *Geocarto Int.* **21**, 21–28.

Sims, D. A., and J. A. Gamon. 2002. Relationships between leaf pigment content and spectral reflectance across a wide range of species, leaf structures and developmental stages. *Remote Sens. Environ.* **81**, 337–354.

Skidmore, A. K., J. G. Ferwerda, O. Mutanga, S. E. Van Wieren, M. Peel, R. C. Grant, et al. 2010. Forage quality of savannas—simultaneously mapping foliar protein and polyphenols for trees and grass using hyperspectral imagery. *Remote Sens. Environ.* **114**, 64–72.

Starks, P. J., S. W. Coleman, and W. A. Phillips. 2004. Determination of forage chemical composition using remote sensing. *Rangel. Ecol. Manag.* **57**, 635–641.

Strobl, C., A.-L. Boulesteix, A. Zeileis, and T. Hothorn. 2007. Bias in random forest variable importance measures: illustrations, sources and a solution. *BMC Bioinformatics* **8**, 25.

Tamm, T., K. Zalite, K. Voormansik, and L. Talgre. 2016. Relating Sentinel-1 interferometric coherence to mowing events on grasslands. *Remote Sens.* **8**, 802.

Tong, A., and Y. He. 2017. Estimating and mapping chlorophyll content for a heterogeneous grassland: comparing prediction power of a suite of vegetation indices across scales between years. *ISPRS J. Photogramm. Remote Sens.* **126**, 146–167.

Valkó, O., S. Venn, M. Żmihorski, I. Biurrun, R. Labadessa, and J. Loos. 2018. The challenge of abandonment for the sustainable management of Palaearctic natural and semi-natural grasslands. *Hacquetia* **17**, 5–16.

Van Wieren, S. E. 1995. The potential role of large herbivores in nature conservation and extensive land use in Europe. *Biol. J. Linn. Soc.* **56**, 11–23.

Veloso, A., S. Mermoz, A. Bouvet, T. Le Toan, M. Planells, J.-F. Dejoux, et al. 2017. Understanding the temporal behavior of crops using Sentinel-1 and Sentinel-2-like data for agricultural applications. *Remote Sens. Environ.* **199**, 415–426.

Verrelst, J., J. Muñoz, L. Alonso, J. Delegido, J. P. Rivera, G. Camps-Valls, et al. 2012. Machine learning regression algorithms for biophysical parameter retrieval: opportunities for Sentinel-2 and-3. *Remote Sens. Environ.* **118**, 127–139.

Voormansik, K., T. Jagdhuber, A. Olesk, I. Hajnsek, and K. P. Papathanassiou. 2013. Towards a detection of grassland cutting practices with dual polarimetric TerraSAR-X data. *Int. J. Remote Sens.* **34**, 8081–8103.

Voormansik, K., T. Jagdhuber, K. Zalite, M. Noorma, and I. Hajnsek. 2016. Observations of cutting practices in agricultural grasslands using polarimetric SAR. *IEEE J. Sel. Top. Appl. Earth Obs. Remote Sens.* **9**, 1382–1396.

Wachendorf, M., T. Fricke, and T. Möckel. 2017. Remote sensing as a tool to assess botanical composition, structure, quantity and quality of temperate grasslands. *Grass Forage Sci.*.

Wang, L., X. Zhou, X. Zhu, Z. Dong, and W. Guo. 2016. Estimation of biomass in wheat using random forest regression algorithm and remote sensing data. *Crop J.* **4**, 212–219.

Wang, J., X. Xiao, R. Bajgain, P. Starks, J. Steiner, R. B. Doughty, et al. 2019. Estimating leaf area index and aboveground biomass of grazing pastures using Sentinel-1, Sentinel-2 and landsat images. *ISPRS J. Photogramm. Remote Sens.* **154**, 189–201.

Warren, S. D., and R. Büttner. 2008. Active military training areas as refugia for disturbance-dependent endangered insects. *J. Insect Conserv.* **12**, 671–676.

Warren, S. D., M. Alt, K. D. Olson, S. D. Irl, M. J. Steinbauer, and A. Jentsch. 2014. The relationship between the spectral diversity of satellite imagery, habitat heterogeneity, and plant species richness. *Ecol. Inform.* **24**, 160–168.

Wilson, J. B., R. K. Peet, J. Dengler, and M. Pärtel. 2012. Plant species richness: the world records. *J. Veg. Sci.* **23**, 796–802.

Wright, M. N., and A. Ziegler. 2015. ranger: a fast implementation of random forests for high dimensional data in C++ and R. ArXiv Prepr. ArXiv150804409.

Yoder, B. J., and R. E. Pettigrew-Crosby. 1995. Predicting nitrogen and chlorophyll content and concentrations from reflectance spectra (400–2500 Nm) at leaf and canopy scales. *Remote Sens. Environ.* **53**, 199–211.

Zalite, K., O. Antropov, J. Praks, K. Voormansik, and M. Noorma. 2016. Monitoring of agricultural grasslands with time series of X-band repeat-pass interferometric SAR. *IEEE J. Sel. Top. Appl. Earth Obs. Remote Sens.* **9**, 3687–3697.

Zandler, H., A. Brenning, and C. Samimi. 2015. Quantifying dwarf shrub biomass in an arid environment: comparing empirical methods in a high dimensional setting. Remote Sens. Environ. 158, 140–155.mental stages. *Remote Sens. Environ.* **81**, 337–354.

Zeng, L., and C. Chen. 2018. Using remote sensing to estimate forage biomass and nutrient contents at different growth stages. *Biomass Bioenerg.* **115**, 74–81.

Supporting Information

Additional supporting information may be found online in the Supporting Information section at the end of the article.

Table S1. A list of spectral predictor variables and the respective groups included in the variable selection process.

Table S2. A list of spectral biophysical predictor variables (L2B) included in the variable selection process.

Table S3. A list of radar predictor variables included in the variable selection process.

Figure S1. Spatial predictions of oADF, CP, CSH and DM for August 2016 and May 2017 using random forest regression, averaged over 100 repetitions.

Figure S2. Spatial predictions of oADF, CP, CSH and DM for August and October 2016 using random forest regression, averaged over 100 repetitions.

